

# Calorimetric and Microstructural Investigation of Frozen Hydrated Gluten

V. Kontogiorgos · H. D. Goff

Published online: 14 November 2006  
© Springer Science+Business Media Inc. 2006

**Abstract** The thermal and microstructural properties of frozen hydrated gluten were studied by using differential scanning calorimetry (DSC), modulated DSC, and low-temperature scanning electron microscopy (cryo-SEM). This work was undertaken to investigate the thermal transitions observed in frozen hydrated gluten and relate them to its microstructure. The minor peak that is observed just before the major endotherm (melting of bulk ice) was assigned to the melting of ice that is confined to capillaries formed by gluten. The Defay–Prigogine theory for the depression of melting point of fluids confined in capillaries was put forward in order to explain the calorimetric results. The pore radius size of the capillaries was calculated by using four different empirical models. Kinetic analysis of the growth of the pore radius size revealed that it follows first-order kinetics. Cryo-SEM observations revealed that gluten forms a continuous homogeneous and not fibrous network. Results of the present investigation showed that it is impossible to assign a  $T_g$  value for hydrated frozen gluten because of the wide temperature range over which the gluten matrix vitrifies, and therefore the construction of state diagrams is not feasible at subzero temperatures for this material. Furthermore, the gluten matrix is deteriorated with two different mechanisms from ice recrystallization, one that results from the growth of ice that is confined in capillaries and the other from the growth of bulk ice.

**Keywords** Differential scanning calorimetry · Frozen dough · Cryo-scanning electron microscopy · Gluten · Recrystallization · Microstructure · Capillary · Porosimetry · Thermoporometry

V. Kontogiorgos · H. D. Goff (✉)  
Department of Food Science, University of Guelph,  
Guelph, ON, Canada, N1G2W1  
e-mail: dgoff@uoguelph.ca

## Introduction

The influence of freezing and frozen storage on the properties of doughs is an area of active research interest with a view to improve the quality of the final thawed product. Common findings among researchers are reduced bread volume, longer proof times, and alteration of the textural characteristics of the baked product. The causes of deterioration are loss of yeast viability and weakening of the strength of the gluten network due to release of reducing substances from the dead yeast cells and to formation of ice crystals.<sup>1–7</sup> The formation of ice is unavoidable and there is a consensus among researchers that the growth of ice crystals during frozen storage (i.e., recrystallization) damages the gluten network resulting in reduced CO<sub>2</sub> retention capacity.

Thermal analysis is frequently used for studying frozen doughs.<sup>8–11</sup> Differential scanning calorimetry (DSC) can be applied to estimate the amount of frozen water and follow several thermal events, such as glass transition temperatures or devitrification. Recently, a study by Bot<sup>9</sup> showed that the thermograms of frozen hydrated gluten and nonyeasted dough consist of two thermal events: a minor peak followed immediately by a major peak. The major peak was assigned to the melting of ice, whereas the minor peak to an enthalpy relaxation that appears after the putative glass transition. However, Johari and Sartor,<sup>12–16</sup> studying several high water content protein systems at subzero temperatures—including myoglobin, hemoglobin, lysozyme, beef, and gluten proteins, have shown that hydrated proteins vitrify and become glassy on cooling in a manner that causes their vitrification region to spread out over a broad temperature range, up to 200°. They attributed this phenomenon to the interactions of water with the protein. These interactions add to the complexity of the atom–atom interactions within the hydrated structure having as a result that the configurational (intermolecular) energy barriers to segmental and group motions

in their hydrated state have exceptionally broad distribution. Consequently, the shape of the endotherm and the determination of  $T_g$  become ambiguous. In the area of food research, the importance of state diagrams to predict food stability is well documented<sup>17</sup> and efforts have been made to predict the  $T_g$  of gluten components with extrapolations from the Gordon–Taylor equation to subzero temperatures.<sup>9,18</sup> However, it is uncertain, because as stated earlier hydrated gluten does not have a sharp  $T_g$  below zero, if the creation of state diagrams for gluten at subzero temperatures is possible.

The generally accepted view of the microstructure of gluten is that hydrated gluten protein molecules interact with each other, thus forming a fibrous three-dimensional network<sup>19,20</sup> that is responsible for the rheological properties of dough.<sup>21–23</sup> Conventional scanning electron microscopy (SEM) observations of dough and gluten,<sup>24–26</sup> cryo-SEM<sup>3,27–31</sup> examination of dough as well as confocal scanning laser microscopy investigations<sup>32–34</sup> of dough and gluten revealed a gluten network at a micron scale. However, the three-dimensional fibrous network of gluten could not be observed by environmental SEM (ESEM),<sup>35,36</sup> which revealed a continuous gluten phase with collapsed structure. As is evident, the view for the microstructure of hydrated gluten is not yet conclusive. Although cryo-SEM has been used to study the microstructure of dough, to the best of our knowledge it has not been used for microstructural observations of frozen hydrated gluten.

Fluids confined in pores exhibit physical properties different than the properties of the bulk fluid (i.e., fluid not constrained in pores).<sup>37</sup> For water confined in pores, its phase change is not a direct result of undercooling.<sup>38</sup> At temperatures below the bulk freezing point (i.e., freezing point of water that is not contained in the pores), confined water can remain unfrozen. Thus, surface tension governs the crystallization process along with the pore-size radius distribution. Foods are porous materials and a fundamental approach for the understanding of the phase change in water has escaped attention. A fundamental understanding of water behavior in such systems could lead to improved formulations and processing conditions resulting in products of superior quality. Below, we describe the theory used in this study to investigate the thermal transitions of frozen hydrated gluten.

### Theoretical aspects

Defay and Prigogine<sup>38</sup> have established a theoretical background for the phase behavior of a liquid held inside a porous material taking into account the effect of curvature of the interfaces. In classical thermodynamics of the equilibrium between two phases, it is supposed that the interface is infinitely flat and all molecules have the same probability to cross the interface from one phase to another. However, if

the interface is curved, the ability of the molecules to diffuse from one phase to another is directly related to the local curvature of the interface. The interfacial pressure and the difference in pressure across the interface have to be considered. The magnitude of curvature depends on the pore size distribution of the material.

The frozen gluten network will be considered as a porous matrix where after hydration the pores are filled with water (confined water) and are surrounded by ice (bulk ice) (Figure 1). Hereafter, this model will be used to interpret thermal events and the state of water in frozen gluten. Defay and Prigogine<sup>38</sup> gave detailed information for the effect of curvature for several different cases. However, the present case, that is, a pore that has been completely filled by water and is surrounded by ice, was not explicitly analyzed. The explicit derivation of this case is given in [Appendix](#). After the analysis the following equation is obtained:

$$T = T_0 - \frac{V_1 \kappa_{sl} \gamma_{sl}}{\Delta H_f} T_0 \quad (1)$$

where  $T$  is the melting temperature of the confined ice,  $T_0$  is the melting temperature of the bulk ice (detailed explanation of the terms is given in [Appendix](#)). Equation (1) shows that further growth of an ice crystal into the narrow capillary cannot occur until the temperature is lowered to  $T$ . This means that water in the capillaries will exhibit a lower melting point than bulk water (i.e., the nonconfined water). Furthermore, it describes the dependence of this temperature ( $T$ ) from the curvature of the interface; that is, the higher the value of the shape factor,  $\kappa_{sl}$ , the lower the new equilibrium temperature. In other words, the smaller the radius of the capillary, the lower the melting point of the confined water. These are the two core concepts of the present work.

The objectives of the present work were to investigate the thermodynamic origin of the thermal transitions of frozen hydrated gluten, to study its microstructure using cryo-SEM, and to explore the applicability of the Defay–Prigogine (DP) theory in the phase behavior of water in frozen hydrated gluten.

### Materials and methods

#### Sample preparation

Gluten, sucrose, and NaCl were purchased from Sigma-Aldrich (St. Louis, MO, USA). For the preparation of hydrated gluten, gluten powder (40% w/w) was mixed with water (or the sucrose or NaCl solutions), and kneaded manually with a spatula until a uniform matrix was obtained. The gluten preparation was left for complete hydration at 4°C for 30 min. Hydrated gluten samples were also prepared with 0.1%, 1%, and 2% w/v NaCl, and 0.58%, 5.88%, and

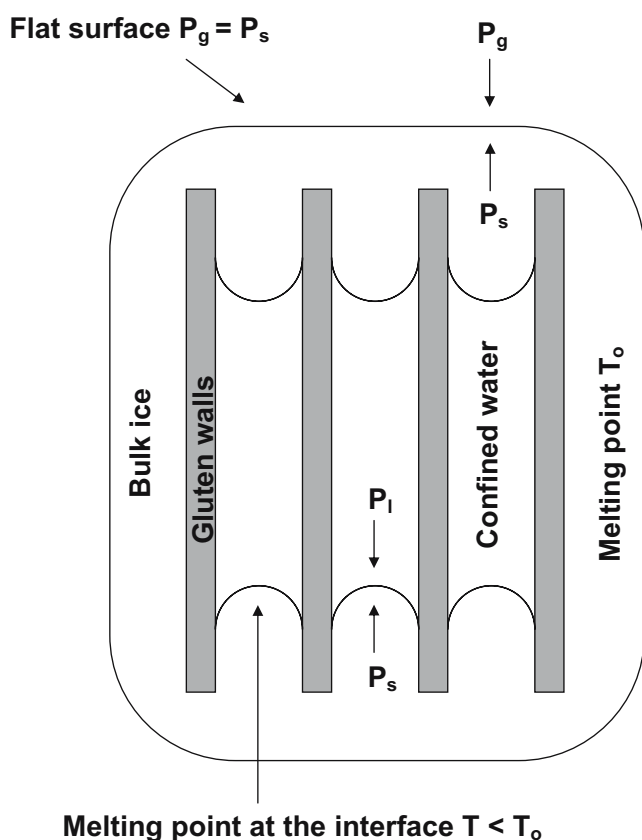


**Fig. 1.** Proposed model for the state of water in hydrated frozen gluten. Variables are explained in [Appendix](#).

11.69% w/v of sucrose. The concentrations of the sucrose solutions were selected so as to exhibit the same melting point depression as the NaCl solutions. To that end, the classic equation for the depression of melting point was used ( $\Delta T = k_f m$ ). The cryoscopic constant  $k_f$  for water equals to  $1.86 \text{ kmol}^{-1} \text{ kg}^{-1}$ , and  $m$  is the molality of the solution. MilliQ water was used for sample preparation.

#### Differential scanning calorimetry

Samples (15–25 mg) were hermetically sealed in Alod-Al pans, and subjected to DSC measurements (Q1000 DSC; TA Instruments, New Castle, DE, USA). The cooling unit was a refrigerated cooling system (RCS) that accompanies the DSC. It operates from  $-90$  to  $550^\circ\text{C}$  using a two-stage, closed evaporative system.  $T_{\text{zero}}$  calibration was performed by heating the cells without pans in the temperature range of interest. Cell constant and temperature calibration was performed with indium and MilliQ water with heating rates of 1 or  $5^\circ\text{C}/\text{min}$  and heat capacity was calibrated using sapphire. For all scans, an empty pan was used as a reference and nitrogen as a purge gas at a flow rate of 50 mL/min. Modulated DSC (MDSC) measurements were performed after quench ( $10^\circ\text{C}/\text{min}$ ) or slow ( $1^\circ\text{C}/\text{min}$ ) cooling of the samples to  $-80^\circ\text{C}$ . The pans were maintained at  $-80^\circ\text{C}$  for

5 min and scanned to  $10^\circ\text{C}$  with underlying heating rate of either 1 or  $5^\circ\text{C}/\text{min}$ , with a period of 60 s, and an amplitude of  $\pm 1^\circ\text{C}$ . To study the effect of cooling rate on the thermal transitions of gluten, the samples were cooled to  $-20^\circ\text{C}$  at 10, 1, 0.5, 0.2, and  $0.1^\circ\text{C}/\text{min}$ , held for 5 min, and scanned at  $1^\circ\text{C}/\text{min}$  to  $10^\circ\text{C}$ . To study the effect of isothermal annealing above the minor transition, the samples were cooled to  $-20$  at  $1^\circ\text{C}/\text{min}$  heated fast (temperature jump) to the annealing temperature ( $-5$  or  $-2^\circ\text{C}$ , for 4h), cooled slowly ( $0.2^\circ\text{C}/\text{min}$ ) to  $-20^\circ\text{C}$ , and finally scanned at  $1^\circ\text{C}/\text{min}$  to  $10^\circ\text{C}$ . To study the effect of sucrose and NaCl, the samples were cooled to  $-20$  at  $0.2^\circ\text{C}/\text{min}$ , held for 5 min, and scanned at  $1^\circ\text{C}/\text{min}$  to  $10^\circ\text{C}$ . To study the effect of isothermal annealing below the minor transition, the samples were cooled at  $1^\circ\text{C}/\text{min}$  to  $-20^\circ\text{C}$ , heated fast to  $-13^\circ\text{C}$ , held isothermally for 0.5, 4, 8, 18, and 28 h, quench cooled to  $-20^\circ\text{C}$ , held for 5 min, and scanned at  $1^\circ\text{C}/\text{min}$  to  $10^\circ\text{C}$ . All experiments were performed at least four times.

#### Cryo-SEM observations

After the end of hydration period, approximately 10 g of hydrated gluten were wrapped in a plastic membrane, and either stored at  $-13 \pm 1^\circ\text{C}$  for the desired storage period or immersed to liquid nitrogen for direct observation. After 1 or 30 days of storage, the samples were unwrapped and submerged immediately in liquid nitrogen, fractured (under liquid nitrogen), placed in a copper sample holder, and transferred in a cryopreparation unit using a transfer device (Emscope SP2000A Sputter cryo, cryogenic preparation system; Emscope Ltd., Kent, UK). The specimens were again fractured with a blade in the preparation chamber to expose a fresh surface and sublimated at  $-80^\circ\text{C}$  for 30 min. After the end of sublimation, the specimens were gold sputter coated for 2 min and transferred to the cryo-SEM microscope stage (Hitachi S-570 SEM, Hitachi Ltd., Tokyo, Japan). The samples were viewed at 10 kV accelerating voltage. Several representative images were collected at different magnifications from different parts of the specimens.

## Results and discussion

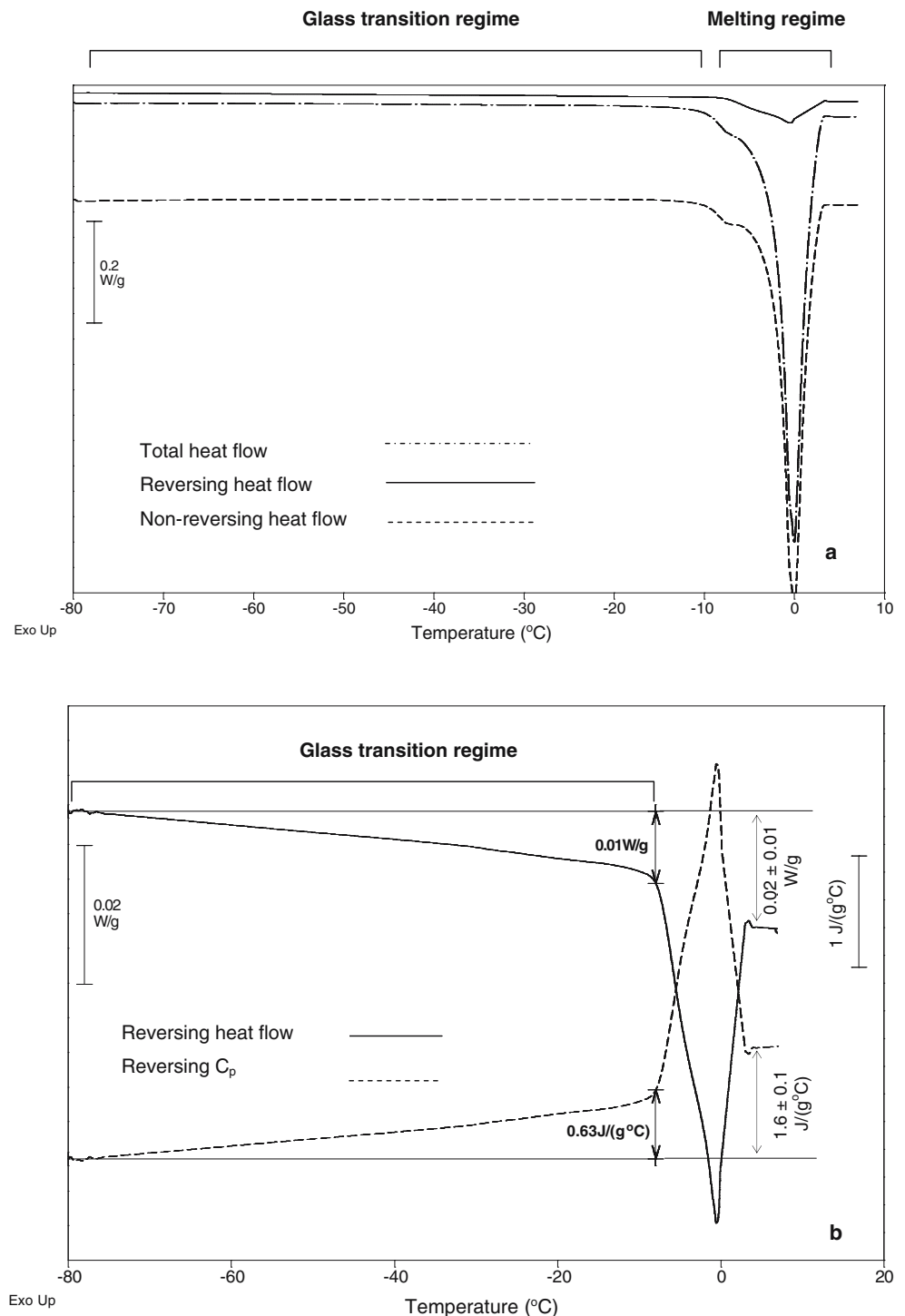
#### Thermal properties of hydrated frozen gluten studied by MDSC

The traces of the total heat flow were similar to those observed by Bot<sup>9</sup>; a minor endothermic event with onset at  $-8.8 \pm 0.5^\circ\text{C}$  followed immediately by the endotherm of ice melting (Figure 2a). After deconvolution of the total heat flow to its components, the minor endothermic peak appeared only in the nonreversing component, which

suggests that this peak is either an enthalpic relaxation peak or a first-order transition. The reversing component depends on the heat capacity of the sample and contains information about the reversible thermodynamic events within the timescale of observation.<sup>39–43</sup> It is usually used to differentiate  $T_g$  (heat capacity dependent) from latent heat of first-order transitions or other nonreversible ther-

modynamic events, such as enthalpic relaxations. The reversing component (Figure 2b) does not appear to contain any definite region that could be assigned to a glass transition temperature of the frozen hydrated gluten. The reversing signal decreases gradually over a large temperature range, from  $-80^\circ\text{C}$  up to the onset of ice melting (Figure 2b). Johari and co-workers,<sup>12–16,44</sup> using standard

**Fig. 2.** MDSC thermograms of hydrated frozen gluten (40% w/w): (a) total, reversing, and nonreversing heat flow; (b) magnification of the reversing heat flow and  $C_p$ . The thermogram consists of a glass transition regime that spans several degrees followed by a melting regime, which is further divided into a small and a large endothermic event.



DSC, observed similar broadness of the endotherm of frozen hydrated gluten. The broadness of the endotherm has been attributed to the complexity of interactions of the protein molecules. Immobilization of the several relaxation elements that comprise a protein (segments associated by H bonds to other proteins, isolated polypeptide chains, or moieties) become gradually mobile upon heating on the experimental timescale that is determined by the heating rate.<sup>13</sup> This also appears as a gradual loss of heat capacity,  $C_p$ , over a broad temperature range<sup>13</sup> (Figure 2b). To verify that the change in magnitude of the reversing heat flow is influenced by kinetics, the transitions were studied under different cooling and heating rates (Figure 3). The cooling rates, i.e., 10 or 1°C/min, did not have any effect on the

transition (not shown). On the other hand, heating rate influenced the magnitude and shape of the transitions (Figure 3a). Fast heating rates correspond to shorter timescales available for relaxation of the immobilized components. Thus, more motions (vibrational, configurational, and translational motions) become kinetically unfrozen and contribute to the change in  $C_p$  in a small period of time, resulting in greater changes in the heat capacity. This set of experiments demonstrated the influence of heating rate on the magnitude of the glass transition region, reinforcing the concept that frozen gluten cannot exhibit a sharp  $T_g$ . The influence of heating rate on the nonreversing component (Figure 3b) showed that the minor endothermic peak cannot be observed with fast heating rates, and this

**Fig. 3.** Effect of heating rate on magnitude of (a) reversing and (b) nonreversing heat flows of frozen hydrated gluten (40% w/w).

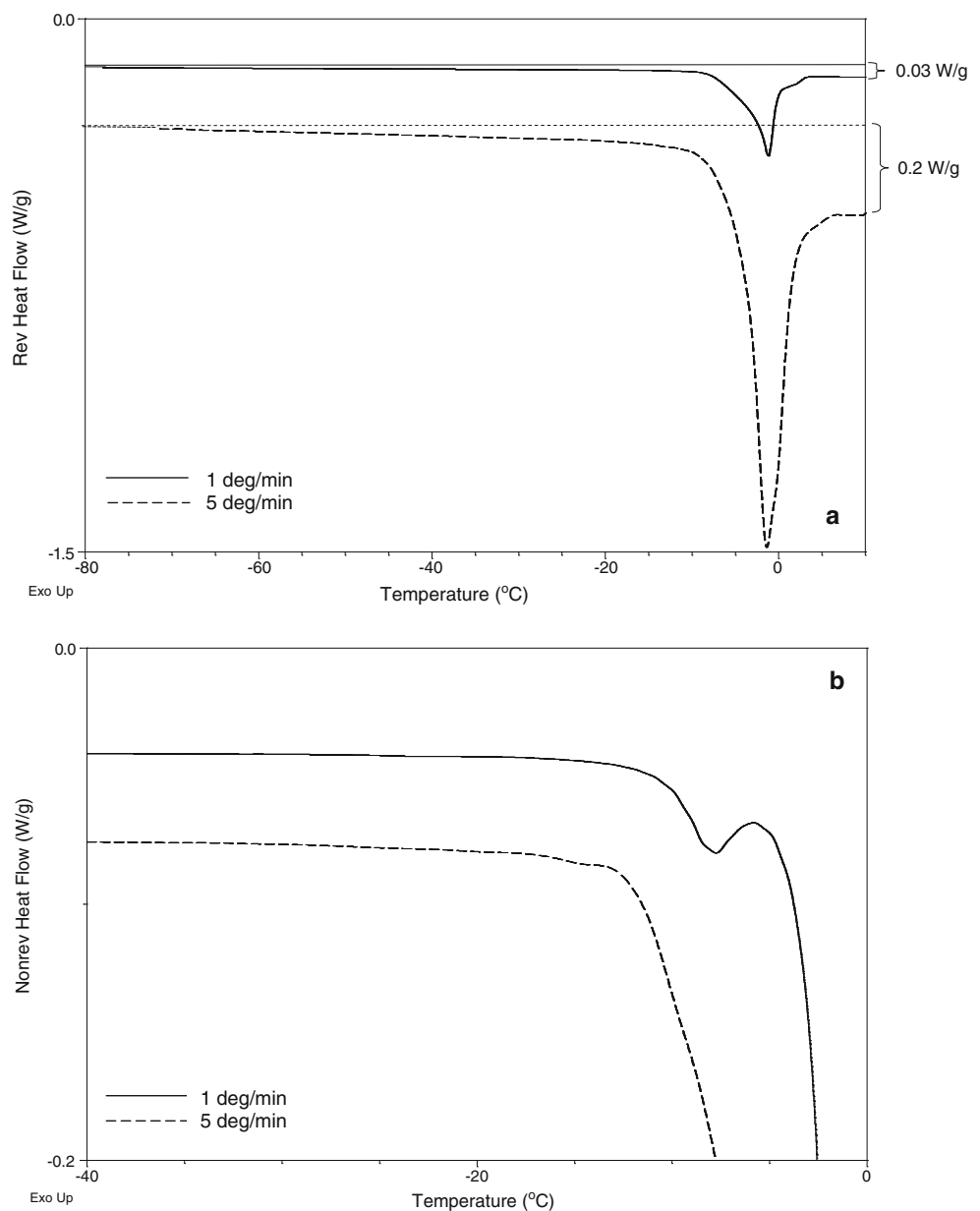
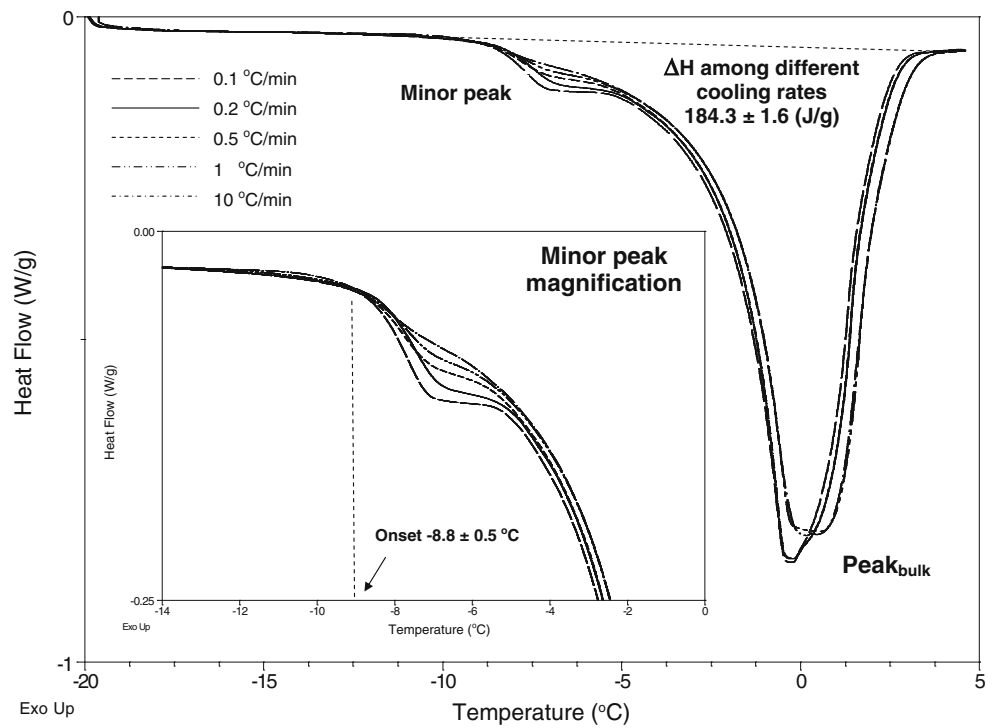


**Fig. 4.** Effect of cooling rate on onset of minor peak in frozen hydrated gluten (40% w/w). Inset shows a magnification of the minor peak with the onset at  $-8.8 \pm 0.5^\circ\text{C}$ .



can be easily explained with the loss of sensitivity of DSC instruments in the separation of overlapping or successive thermal events. Therefore, in order to investigate the complete thermal profile of frozen hydrated gluten, slow heating rates must be employed. It must also be stressed that the selected conditions generate a cooling period during the measurement, which may affect the results and the interpretation of the data. However, we have also

evaluated the effect of heat-only mode with underlying heating rates 2 or 5 °C/min and amplitudes  $\pm 0.318^\circ\text{C}$  or  $\pm 0.796^\circ\text{C}$ , respectively, and the results revealed that the heat-only mode has the same effect as the heat-cool mode used here. However, we worked in the heat-cool mode because the large modulation amplitudes ( $\pm 1^\circ\text{C}$ ) produce large instantaneous heating rates and hence give rise to increased heat flow sensitivity.<sup>40</sup>

**Fig. 5.** Effect of annealing (4 h) in frozen hydrated gluten (40% w/w) at two different temperatures ( $-5^\circ\text{C}$ ,  $-2^\circ\text{C}$ , for 4h). Samples were frozen to  $-20^\circ\text{C}$ , heated to the aging temperature, cooled slowly back to  $-20^\circ\text{C}$ , and heated at  $1^\circ\text{C}/\text{min}$ . The inset shows that the onset of the minor peak remains at  $-8.8 \pm 0.3^\circ\text{C}$ .

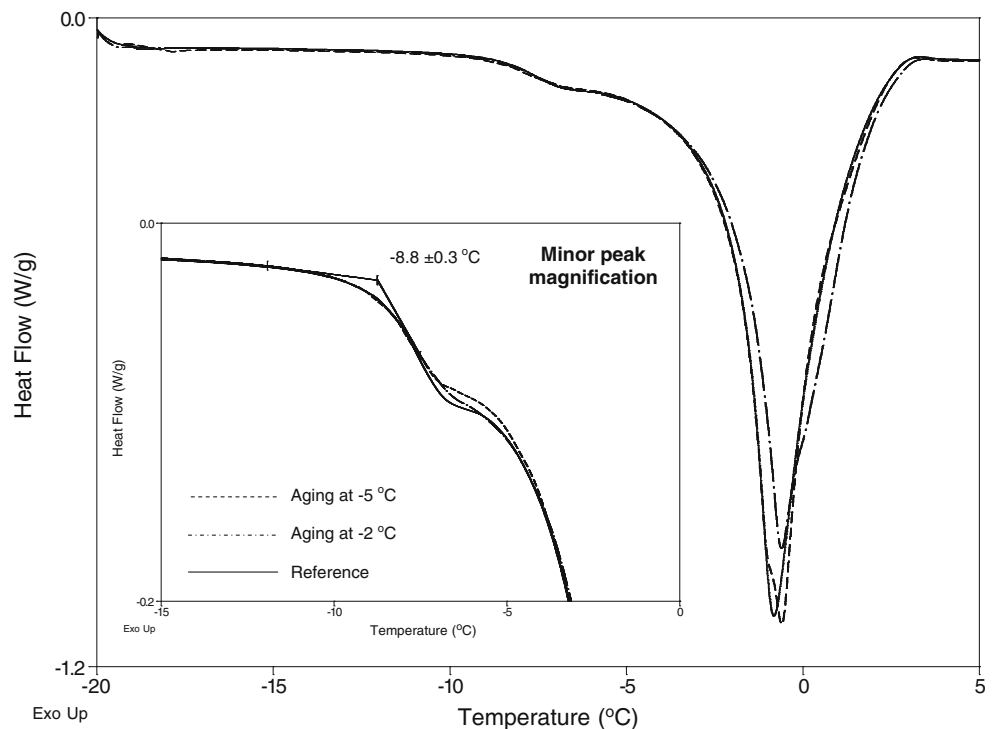
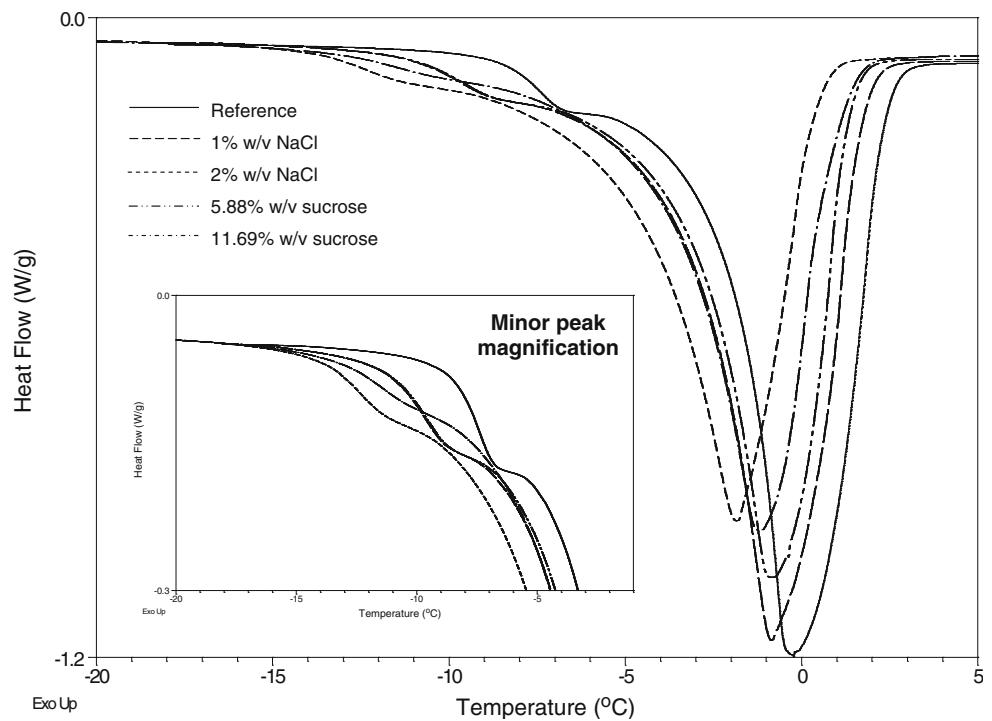


**Fig. 6.** Effect of different concentrations of NaCl and sucrose in frozen hydrated gluten (40% w/w) on the onset and shape of the minor peak. Inset shows a magnification of the onset area.



Thermal properties of hydrated frozen gluten studied by standard DSC

In this set of experiments, classical calorimetric techniques were employed in order to focus on the behavior of the minor peak of the nonreversing component and verify the MDSC results. In the effect of cooling rate on the endotherm (Figure 4), the major peak ( $\text{peak}_{\text{bulk}}$ ) can be easily assigned

to the endotherm of melting of bulk ice. For the minor peak, one could argue that it represents an enthalpic relaxation peak. The effect of cooling rate clearly shows that the minor peak cannot be attributable to a second-order transition because its onset did not vary with the cooling rate ( $8.8 \pm 0.5^\circ\text{C}$ ). Generally, because glass transition is a purely kinetic phenomenon,<sup>45</sup> the cooling rate affects the position of the transition. Furthermore, a glass transition

**Fig. 7.** Effect of isothermal annealing at  $-13^\circ\text{C}$  in frozen hydrated gluten (40% w/w) at several holding periods on the position of  $\text{peak}_{\text{cap}}$ .

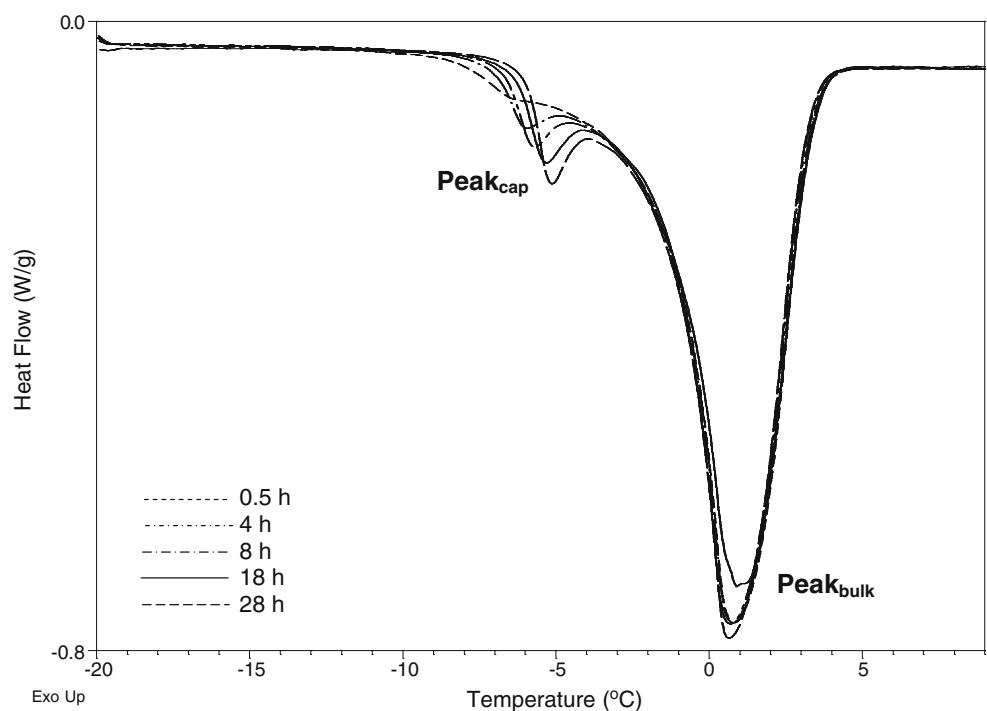


**Table 1** Pore radius size calculations of frozen hydrated gluten (40% w/w) after isothermal annealing at  $-13^{\circ}\text{C}$  for several hours using four different models

Annealing time (h)	Radius (nm)			
	Brun	Landry	Ishikiryama ( $\delta=0.5$ nm)	Ishikiryama ( $\delta=2.2$ nm)
0.5	5.04	3.74	5.31	7.01
4	5.28	3.88	5.56	7.26
8	5.57	4.06	5.86	7.56
18	5.80	4.20	6.10	7.80
28	6.14	4.41	6.44	8.14

Values with in the table are significantly different within columns and rows ( $P>0.05$ ).

event shifts the baseline to a considerably lower level as a result of differences in the heat capacities before and after the transition. However, after the end of both transitions the shift of the baseline was negligible. Examination of the enthalpies of melting (Figure 4) did not show substantial differences among different cooling rates, suggesting that the overall ice content remains relatively constant under the present experimental conditions. If the minor peak were an enthalpic relaxation peak, then  $\Delta H$  values would be significantly different because the enthalpy lost during relaxation would be recovered during heating and would add up to the total enthalpy observed.

Because it was still not clear, within the experimental error of thermal analysis, whether the onset of the peak is affected from the cooling rate, isothermal annealing was needed (Figure 5). The cooling rate to  $-20^{\circ}\text{C}$  from the annealing temperature was selected to be slow ( $0.2^{\circ}\text{C}/\text{min}$ )

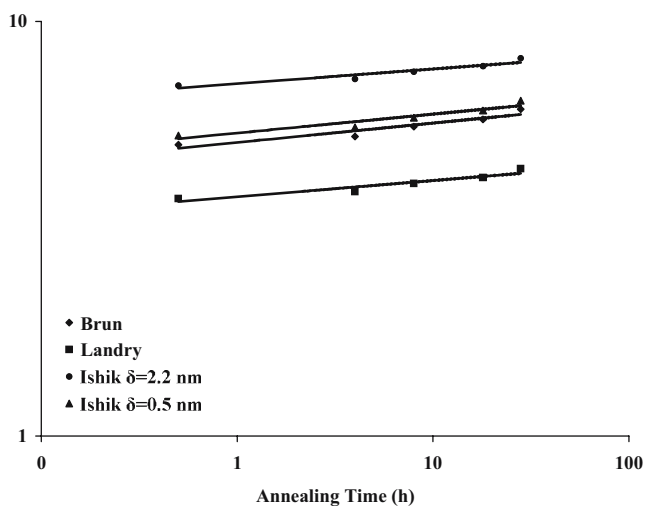


**Fig. 8.** Double logarithmic plots of the kinetics of pore radius growth versus annealing time (at  $-13^{\circ}\text{C}$ ) using four different empirical models.

in order to favor ice crystal growth and avoid secondary nucleation events. The results show that the onset of the peak remained at  $-8.8\pm 0.3^{\circ}\text{C}$  even after the annealing protocol. If the onset of the transition were a glass transition, then the peak would shift to higher temperatures after the extensive annealing that was employed. However, the position of the peak remained unaffected, which argues that this transition is related to a first-order thermal event, i.e., ice melting.

The last step in the investigation of the origin of the minor peak was to study the effect of compounds that can depress the freezing point of water. The onset of the transition was indeed changed from  $-8.8\pm 0.5^{\circ}\text{C}$  to  $-13.5\pm 0.4^{\circ}\text{C}$  with the concentration of the depressant (Figure 6). At high concentrations, 1% w/v for NaCl and 11.69% w/v for sugar, deviation of the curves from one another was observed, which suggests that the transition is no longer solely influenced by the melting point depression and that interactions between proteins may come into play. Nevertheless, all concentrations studied had a dramatic effect on the shape and position of the minor peak.

MDSC and standard DSC experiments showed strong evidence that the minor peak is exclusively related to the melting of ice, and that hydrated gluten does not exhibit a finite  $T_g$  temperature. The latter has important consequences because it renders the creation of state diagrams at subzero temperatures unfeasible for hydrated gluten. Moreover, the construction of such diagrams assumes solubility of the compound and that the system is homogeneous irrespective of the mass volume fraction. The construction of a state diagram for hydrated gluten needs also to take into account the water-insoluble behavior of gluten. Therefore, the physical sense of  $T_g$  of hydrated gluten is questionable. Additionally, the results propose that the stability of frozen doughs at subzero temperatures increases gradually and continuously over a wide range of decreasing temperatures, as the kinetics of structural molecular rearrangements changes during the slow vitrification process in the gluten network. Real dough formulations also contain other ingredients, including starch, yeasts, salt, sugar, shortening, and other minor components embedded in the gluten matrix. These can also undergo vitrification, so efforts to achieve longer storage stability of frozen dough must take into account the stability of the freeze-concentrated phase in the context of the stability of the gluten network described above. Rasanen et al.<sup>11</sup> and Laaksonen and Roos<sup>10,46</sup> observed  $T_g'$  temperatures for flour–water mixtures of several different formulations in the range of  $\sim -40$  to  $\sim -25^{\circ}\text{C}$  using dynamic mechanical thermal analysis (DMTA), dynamic mechanical analysis (DMA), and dielectric analysis (DEA) as analytical tools. However, the present study suggests that the contribution of gluten to the signals they observed should not be the



**Table 2** Kinetic parameters of the dependence of pore radius with annealing time

	$\alpha$	$\beta$	$r^2$
Brun	5.1	0.046	0.90
Landry	3.7	0.039	0.91
Ishik. ( $\delta=0.5$ nm)	5.3	0.045	0.90
Ishik. ( $\delta=2.2$ nm)	7.1	0.035	0.92

Parameter  $\alpha$  represents the pore radius dimension at zero annealing time, whereas  $\beta$  shows the growth rate of the pore radius.

dominant one and the contributions from starch and other components must be taken into consideration.

Peaks such as the minor peak seen here have been observed by using a plethora of different porous materials and confined liquids.<sup>47–59</sup> The common observation is a minor peak that is assigned to the melting of confined crystals, followed by a major thermal event that is assigned to the melting of bulk crystals. What follows then is an analysis of the assignment of the minor peak to confined water in capillaries of the hydrated gluten network, hence the designation of the minor peak as capillary water, peak<sub>cap</sub>.

#### Application of Defay–Prigogine theory—estimation of the pore diameter

It has been stated<sup>15</sup> that because DP theory<sup>38</sup> has been developed assuming that the pore walls are rigid and there is no interaction between the confined liquid molecules and the wall, it cannot be applied to hydrated proteins, because protein walls are not rigid and they interact with water. However, it has been shown that in systems with rigid walls there is always a layer of nonfreezable water in equilibrium with ice.<sup>60,61</sup> In gluten, a monomolecular water layer interacts with gluten, mostly by hydrogen bonding, and remains unfreezable.<sup>62</sup> Therefore, in both cases, a thin layer of water is always in equilibrium with the ice, and ice cannot interact directly with other hydrophilic groups (–OH, –NH) of gluten. This layer has thickness  $\delta$  and is important for very small pores, as will be discussed below. As for the crystallization in porous media with nonrigid surface, Coussy<sup>63</sup> has shown that the principles of DP theory can be applied to confined liquids in porous media with deformable walls.

In an effort to investigate the behavior of peak<sub>cap</sub> due to storage at temperatures below the onset of peak<sub>cap</sub>, isothermal annealing at  $-13^\circ\text{C}$  was performed. The cooling rate was selected to be  $1^\circ\text{C}/\text{min}$  because this rate does not create an evident peak<sub>cap</sub> (Figure 4). Therefore, all the differences could be easily attributed to the effect of isothermal holding. The temperature was selected to be

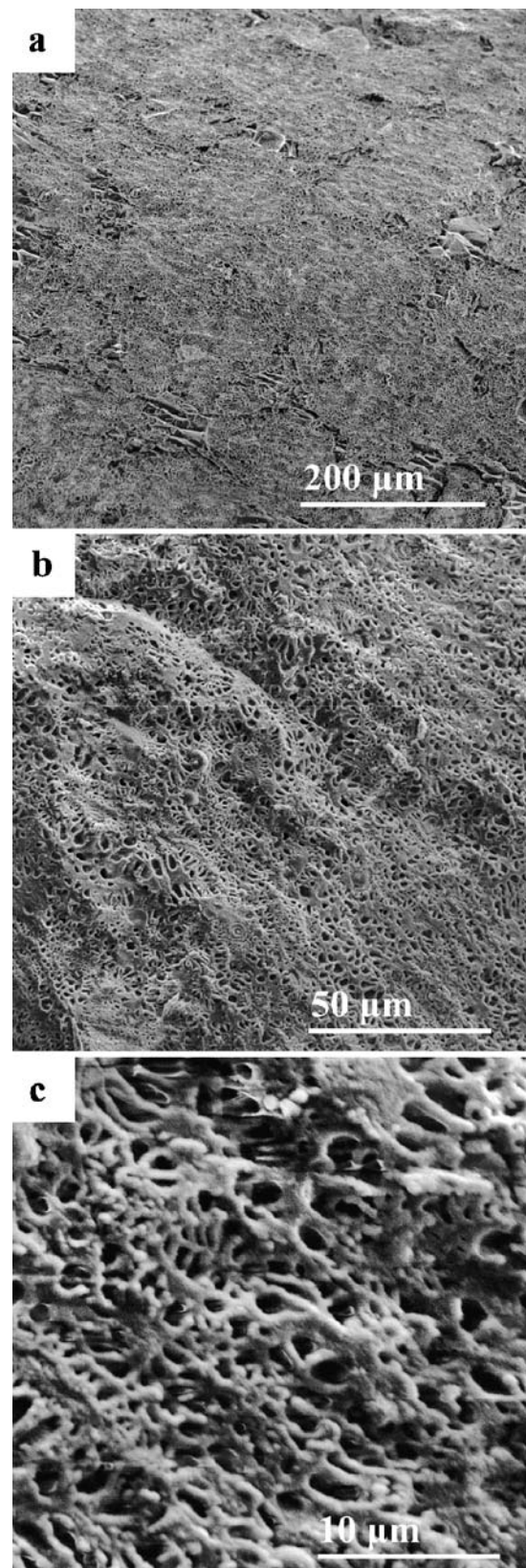


**Fig. 9.** Images of frozen hydrated gluten (40% w/w) taken with cryo-SEM immediately after the end of hydration period. Porosity of the structure is evident especially at higher magnifications. Bars (a) 200, (b) 50, and (c) 10  $\mu\text{m}$ .

below the onset of the  $\text{peak}_{\text{cap}}$  but high enough to allow for molecular motion and observation of differences at a reasonable experimental timeframe. The measurements showed that the longer the sample is kept, the greater is the magnitude of  $\text{peak}_{\text{cap}}$  (Figure 7). A shift in the onset temperature of  $\text{peak}_{\text{cap}}$  to higher temperatures can also be observed. Bot<sup>9</sup> has observed similar trends after 2 months of storage under constant temperature. To explain such a behavior, several theories are available to describe the solidification processes in a porous body. The most popular include (a) nucleation, where the solidification occurs from nuclei that appear and grow as the temperature decreases; (b) penetration of the solid front, where the solidification proceeds by progressive penetration of the solid phase formed outside the pores; and (c) combination of both of the above.<sup>61,64,65</sup> For now, none of the above mechanisms can be excluded and case (c) seems to be more appropriate for the present system. Once the crystal has entered the pore (the conditions for a crystal to enter a pore have been described elsewhere in detail<sup>65,66</sup>) or the confined water has been expanded due to solidification, ice exerts stresses on the pore walls. These stresses are able to damage the pores, merge two adjacent small pores to one greater, and increase their effective radius. Therefore, according to Eq. (1), the melting point of the water confined in the capillaries shifts to higher temperatures. Thus, the longer the sample is stored, the more the ice grows in the capillaries and impairs the gluten network. The above observations identify the damage of the network that is coming from the ice confined in the pores to be a source of gluten deterioration.

The next step in the investigation was to estimate the pore diameter from available empirical models that have been extensively used to estimate the pore size diameter of model<sup>48,50,51,64</sup> and “real”<sup>49,53,56</sup> porous systems. The assumption used in these models is that the pore shape is cylindrical. There is no evidence that gluten pores are exclusively of cylindrical shape; nevertheless, this assumption was adopted as a starting point in the present

investigation. The empirical models describing the melting point depression with the pore radius diameter that were used were as follows:

$$\text{Brun model}^{64}: r = -\frac{32.33}{\Delta T} + 0.68$$

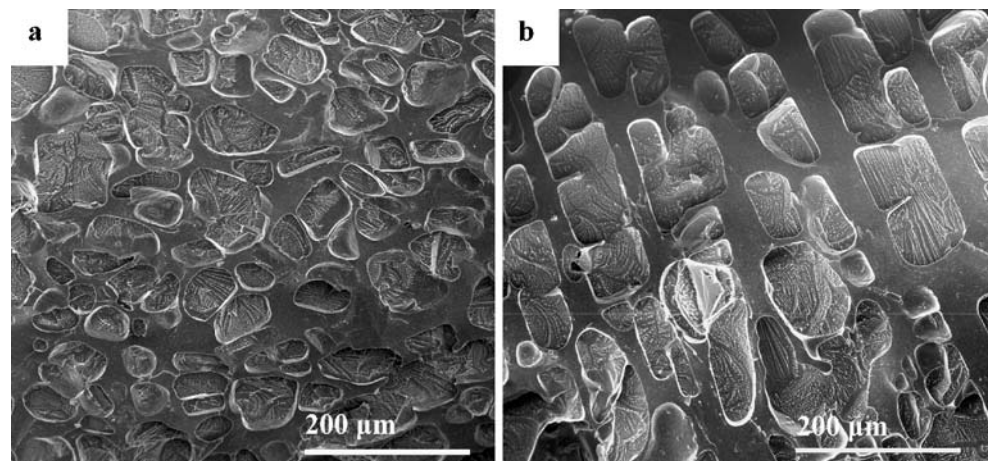
$$\text{Landry model}^{50}: r = -\frac{19.082}{\Delta T + 0.1207} + 1.12$$

$$\text{Ishikiriyama model}^{67,68}: r = -\frac{33.30}{\Delta T} + 0.32 + \delta$$

where  $r$  is the pore radius (nm),  $\Delta T$  is the freezing point depression, and  $\delta$  is the thickness of the layer of water that remains unfrozen and its value for the last model varies between  $0.5 \text{ nm} < \delta < 2.2 \text{ nm}$ .

All models predict similar behavior: high melting point depression for small pore sizes that quickly decreases and eventually converges to the bulk melting temperature after approximately 1000 nm radius size. Data such as those in Figure 7 were used to calculate the pore size increment with isothermal annealing time. The difference of the  $\text{peak}_{\text{cap}}$ - $\text{peak}_{\text{bulk}}$  of the transitions was taken in order to calculate  $\Delta T$  as suggested by Landry. It must be noted that as written, the values of  $\Delta T$  are negative, reflecting that the pore transition temperatures are lower than the bulk value.<sup>50</sup> After  $\Delta T$  evaluation, it was found to range between 7.5 degrees and 5.8 degrees. This range compares reasonably well to water melting point depression in other porous materials, e.g., 12.5–6.5° for PHPMA hydrogel,<sup>48</sup> 10° for cross-linked dextran,<sup>69</sup> 4–5° for cellulose films,<sup>53</sup> or 1–20° for a wide range of controlled pore glasses.<sup>50,70</sup> Analysis of variance revealed that all radii calculated were significantly different among different annealing times and different models (Table 1). Double logarithmic plots (Figure 8) of the pore radius against annealing time revealed a straight line typical of first order processes ( $r = \alpha t^\beta$ ). The parameter  $\alpha$  in the model represents the pore radius at zero annealing time, which is the time at the end of the hydration period. Parameter  $\beta$  shows the rate of growth of the pore radius with annealing time. The Ishikiriyama ( $\delta = 2.2 \text{ nm}$ ) and Landry yield slower while Brun and Ishikiriyama ( $\delta = 0.5 \text{ nm}$ ) models faster growth rates (Table 2). It should be

**Fig. 10.** Images of frozen hydrated gluten (40% w/w) taken with cryo-SEM after (a) 1 day and (b) 30 days of storage. The engraved textures are assigned to the place where ice crystals were taken before the sublimation. Ice crystal growth during storage due to recrystallization of ice is also evident. Bar = 200  $\mu\text{m}$ .



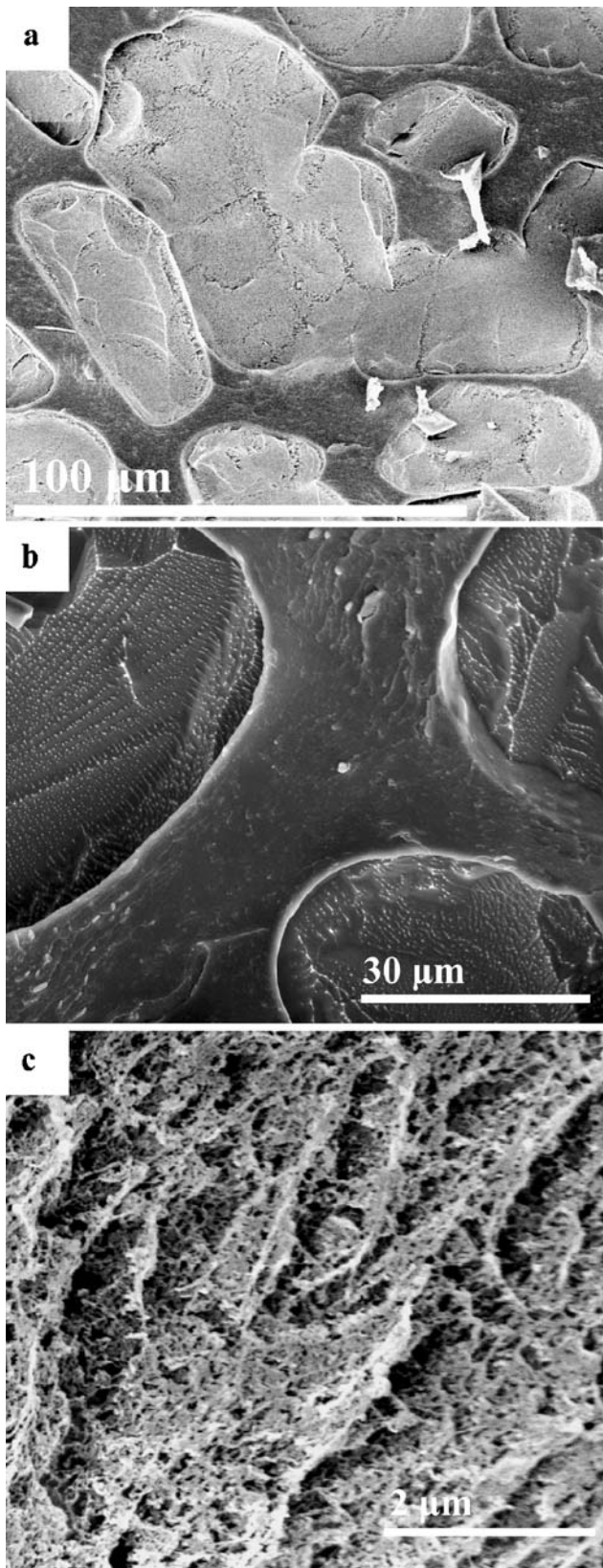


**Fig. 11.** Images of frozen hydrated gluten (40% w/w) taken with cryo-SEM at higher magnifications after 1 day of storage. The structure is homogeneous and the absence of a fibrous network is evident at all scales studied. Bars=(a) 100, (b) 30, and (c) 2  $\mu\text{m}$ .

noted that below 20 nm, subtle differences in pore radius size result in large differences in the melting point depression as is predicted from the models. It must be stressed, however, that we cannot conclude which of the models describes better the porosity of the gluten network. Further research is needed using different techniques (e.g., mercury or nitrogen adsorption porosimetry) in order to identify which of the models provides a better description of the present system. Nevertheless, DP theory seems to apply and has the power to interpret thermal transitions observed in frozen hydrated gluten.

#### Microstructure

Figure 9 shows cryo-SEM micrographs of hydrated gluten that were immersed to liquid nitrogen immediately after preparation without frozen storage. The fast cooling rates used under these conditions do not allow the formation of evident ice crystals. This allows observation of a structure that closely corresponds to the original, i.e., before freezing. The structure appears to be homogeneous at low magnifications (Figure 9a), whereas at higher magnifications (Figure 9b,c) the porosity of the structure is evident. The gluten walls form a perforated network that is able to create a continuous macroscopic structure.

Figure 10 depicts an overall view of the microstructure at a low magnification, 1 day and 30 days after storage. Two phases can now be observed, a continuous gluten phase surrounding the dispersed ice crystals. The irregular, round-etched shapes correspond to the place where ice crystals were located before sublimation. The slow cooling rates used during freezing at  $-13^{\circ}\text{C}$  allow for ice crystal formation. This observation is very important because it stresses the influence of cooling rate on the microstructure of frozen hydrated gluten. The formation of ice crystals results in compression of the structure, something that will probably play a major role on the mechanical properties of frozen dough-based products. The growth of ice crystal size due to ice recrystallization after 30 days of storage is also apparent (Figure 10b). Closer inspection of the surface at higher magnifications confirmed the continuity of the structure (Figure 11). The surface of areas beneath ice crystals was coarser (Figure 11c) compared to the smooth that separates adjacent ice crystals (Figure 11b). This smooth region (Figure 11b) probably occurs after compression of the network as a result of ice crystal formation. However, at all magnifications and cooling rate conditions studied, the fibrous network suggested by other researchers could not be observed.

The model proposed from studies using ESEM<sup>35,36</sup> is that gluten forms into sheets as opposed to fibers. Bache and Donald<sup>35</sup> proposed that a fibrous network might exist at shorter length scale, i.e., at the molecular level. Cryo-

SEM is advantageous compared to ESEM in that it preserves the structure formed after the end of hydration or storage period since the sample observation proceeds continuously under frozen conditions. Sublimation etches the surface, allowing examination of the “frozen-in” gluten microstructure. Another advantage it holds when compared to ESEM is the higher magnifications that can be achieved, allowing closer inspection of the microstructure (Figures 9 and 11). Results of the present study are in general agreement with the model proposed by ESEM observations and do not reveal the existence of a fibrous network at a micron scale. Furthermore, arrangement of gluten in sheets at nanoscale allows more easily conceptualization of a porous structure that is able to depress the melting point compared to the arrangement in fibers (Figure 1). Finally, it appears (Figures 7 and 10) that the gluten network can be deteriorated by two separate mechanisms: one that arises from the growth of ice into the capillaries and the other from the growth of bulk ice crystals. Control of these mechanisms could lead to improvement in the behavior of a real product during storage.

## Conclusions

The thermal and microstructural properties of frozen gluten network have been studied via MDSC, DSC, and cryo-SEM. Calorimetric results showed that it is impossible to assign a finite  $T_g$  value to hydrated gluten at subzero temperatures and therefore the construction of a state diagram is not feasible. The microstructure of gluten was described as a porous body where water can be crystallized in the pores and give rise to a minor peak in the DSC thermograms just before the onset of melting of the bulk ice. To investigate the behavior of the peak, the Defay and Prigogine theory for the depression of the melting point of a liquid confined in pores was applied for the first time to a frozen food system. Description of the microstructure of gluten with this model revealed that the ice confined in pores acts as a secondary source of deterioration of the gluten network along with the growth of the bulk ice. Kinetic analysis of the growth of the pore radius dimension with annealing time revealed that the growth of pore radius follows first-order kinetics. Observations with cryo-SEM revealed that gluten forms a homogeneous network and the proteins at submicron scales are probably arranged in sheets as opposed to fibers.

**Acknowledgments** The authors wish to thank the Greek State Scholarships Foundation and the Natural Sciences and Engineering Research Council of Canada (NSERC) for financial support, and Dr. S. Smith for technical assistance and fruitful discussions regarding the cryo-SEM part of the study.

## Appendix

In the following, a modification of the Kelvin equation for the case of water that is confined in a pore and is surrounded by ice will be derived. The subscripts refer to Figure 1.

For a system in equilibrium with flat surfaces, the Gibbs–Duhem equation for each phase is:

$$-S_i dT + V_i dP_i + n_i d\mu_i = 0 \quad (\text{A1})$$

where  $S_i$ ,  $V_i$ ,  $n_i$ , and  $\mu_i$  are the entropy, volume, number of moles, and chemical potential of phase  $i$  [where  $i$  designates gas (g), liquid (l) or solid (s)].

The system must also be in mechanical equilibrium and therefore the Laplace equation for the solid liquid interface is:

$$P_s - P_l = \kappa_{sl} \gamma_{sl} \quad (\text{A2})$$

where  $\kappa_{sl}$  is a shape factor that relates to the interface curvature between solid and liquid phases and  $\gamma_{sl}$  the interfacial tension between the solid and liquid interfaces.

Because the solid–gas interface is flat the pressures on each side of the interface will be equal:

$$P_g = P_s \quad (\text{A3})$$

It is also known that at equilibrium the chemical potentials of each phase are equal:

$$n_s \mu_s = n_l \mu_l = n_g \mu_g \quad (\text{A4})$$

If the system passes from one equilibrium state to another neighboring equilibrium state, then:

$$dP_s - dP_l = d(\kappa_{sl} \gamma_{sl}) \text{ or } dP_l = dP_s - d(\kappa_{sl} \gamma_{sl}) \quad (\text{A5})$$

$$dP_g = dP_s \quad (\text{A6})$$

$$n_s d\mu_s = n_l d\mu_l = n_g d\mu_g \quad (\text{A7})$$

It is necessary to find a relation between the thermodynamic parameters that describe the system where all the above equations can be used in the analysis. Since the Gibbs–Duhem (GD) equations for each phase equal to zero at equilibrium, then it is valid to subtract  $GD_{\text{solid}} - GD_{\text{liquid}}$  and  $GD_{\text{gas}} - GD_{\text{solid}}$ . The first subtraction and use of Eqs. (A5), (A6), and (A7) gives:

$$\left( \frac{S_l - S_s}{V_s - V_l} \right) dT + dP_s + \frac{V_l}{V_s - V_l} d(\kappa_{sl} \gamma_{sl}) = 0 \quad (\text{A8})$$

After the second subtraction:

$$\frac{S_s - S_g}{V_g - V_s} dT + dP_s = 0 \quad (\text{A9})$$

A third subtraction of Eqs. (A8) and (A9) yields:

$$\left[ (S_l - S_s) - \frac{V_s - V_l}{V_g - V_s} (S_s - S_g) \right] dT = -V_l d(\kappa_{sl}\gamma_{sl}) \quad (\text{A10})$$

Since  $V_g \gg V_s, V_l$ , and  $V_s - V_l \ll V_g$ , the second term in the square brackets can be neglected. On melting  $\Delta S_{s \rightarrow l} = S_l - S_s$ . The entropy change at equilibrium is  $\Delta S_{s \rightarrow l} = \Delta H_f / T_0$ , where  $\Delta H_f$  is the heat of fusion of ice and  $T_0$  is the equilibrium melting point of bulk water. By utilizing all of the above, one finally arrives at:

$$\frac{dT}{T} = -\frac{V_l d(\kappa_{sl}\gamma_{sl})}{\Delta H_f} \quad (\text{A11})$$

Equation (A11) with integration from  $T_0$  to  $T$  and from 0 to  $\kappa_{sl}\gamma_{sl}$  yields:

$$\ln \frac{T}{T_0} = -\frac{V_l \kappa_{sl}\gamma_{sl}}{\Delta H_f} \quad (\text{A12})$$

Equation (A12) can also be found with a positive sign. This depends on the choice of the curvature (wetting or not wetting of the walls), and the change in curvature remedies this discrepancy. The shape factor can be taken as  $2/r_{sl}$  if it is assumed that the surface is hemispherical.

The logarithm in Eq. (A12) can be approximated by using:

$$\ln \frac{T}{T_0} = \ln \left( 1 + \frac{T - T_0}{T_0} \right) \approx \frac{T - T_0}{T_0} \quad (\text{A13})$$

And finally, Eq. (A12) can be rearranged to:

$$T = T_0 - \frac{V_l \kappa_{sl}\gamma_{sl}}{\Delta H_f} T_0 \quad (\text{A14})$$

## References

- P.D. Ribotta, A.E. Leon and M.C. Anon, *Cereal Chem* **80**, 454 (2003).
- P.D. Ribotta, A.E. Leon and M.C. Anon, *J Agric Food Chem* **49**, 913 (2001).
- P.T. Berglund, D.R. Shelton and T.P. Freeman, *Cereal Chem* **68**, 105 (1991).
- Y. Inoue and W. Bushuk, *Cereal Chem* **68**, 627 (1991).
- Y. Inoue, H.D. Sapirstein, S. Takayanagi and W. Bushuk, *Cereal Chem* **71**, 118 (1994).
- Y. Inoue and W. Bushuk, *Cereal Chem* **69**, 423 (1992).
- K. Autio and E. Sinda, *Cereal Chem* **69**, 409 (1992).
- A. Baier-Schenk, S. Handschin and B. Conde-Petit, *Cereal Chem* **82**, 251 (2005).
- A. Bot, *Cereal Chem* **80**, 366 (2003).
- T.J. Laaksonen and Y.H. Roos, *J Cereal Sci* **32**, 281 (2000).
- J. Rasanen, J.M.V. Blanshard, J.R. Mitchell, W. Derbyshire and K. Autio, *J Cereal Sci* **28**, 1 (1998).
- G.P. Johari, *J Phys Chem B* **101**, 6780 (1997).
- G.P. Johari and G. Sartor, *J Chem Soc Faraday Trans* **93**, 2609 (1997).
- G. Sartor and G.P. Johari, *J Phys Chem B* **101**, 6791 (1997).
- G. Sartor and G.P. Johari, *J Phys Chem B* **101**, 6575 (1997).
- G. Sartor, E. Mayer and G.P. Johari, *Biophys J* **66**, 249 (1994).
- M.-S. Rahman, *Trends Food Sci Technol* **17**, 129 (2006).
- J.L. Kokini, A.M. Cocero, H. Madeka and E. Degraaf, *Trends Food Sci Technol* **5**, 281 (1994).
- R. Laszity, *The Chemistry of Cereal Proteins*, 2nd ed. (CRC Press, Boca Raton, FL 1996), p. 328.
- J.D. Schofield, Flour proteins: structure and functionality in baked products. In: *Chemistry and Physics of Baking*, edited by J.M.V. Blanshard, P.J. Frazier and T. Galliard (Royal Society of Chemistry, London 1986).
- P.S. Belton, *J Cereal Sci* **41**, 203 (2005).
- B.J. Dobraszczyk and M. Morgenstern, *J Cereal Sci* **38**, 229 (2003).
- H. Singh and F. MacRitchie, *J Cereal Sci* **33**, 231 (2001).
- T. Amend and H.D. Belitz, *Z Lebensm -Unters Forsch* **190**, 401 (1990).
- T. Amend, H.D. Belitz, R. Moss and P. Resmini, *Food Struct* **10**, 277 (1991).
- O. Paredeslopez and W. Bushuk, *Cereal Chem* **60**, 24 (1983).
- P.T. Berglund, D.R. Shelton and T.P. Freeman, *Cereal Foods World* **33**, 675 (1988).
- P.T. Berglund, D.R. Shelton and T.P. Freeman, *Cereal Chem* **67**, 139 (1990).
- E. Esselink, H. van Aalst, M. Maliepaard, T.M.H. Henderson, N. L.L. Hoekstra and J. van Duynhoven, *Cereal Chem* **80**, 419 (2003).
- S. Zounis, K.J. Quail, M. Wootton and M.R. Dickson, *J Cereal Sci* **36**, 135 (2002).
- S. Zounis, K.J. Quail, M. Wootton and M.R. Dickson, *J Cereal Sci* **35**, 135 (2002).
- A. Baier-Schenk, S. Handschin, M. von Schonau, A.G. Bittermann, T. Bachi and B. Conde-Petit, *J Cereal Sci* **42**, 255 (2005).
- M.B. Durrenberger, S. Handschin, B. Conde-Petit and F. Escher, *Lebensm-Wiss Technol* **34**, 11 (2001).
- W. Li, B.J. Dobraszczyk and P.J. Wilde, *J Cereal Sci* **39**, 403 (2004).
- I.C. Bache and A.M. Donald, *J Cereal Sci* **28**, 127 (1998).
- A.D. Roman-Gutierrez, S. Guilbert and B. Cuq, *Lebensm-Wiss Technol* **35**, 730 (2002).
- F. Romm, *Microporous Media* (Marcel Dekker, New York 2004).
- R. Defay and I. Prigogine, *Surface Tension and Adsorption* (Longmans, London 1966).
- J.E.K. Schawe, *Thermochim Acta* **304–305**, 111 (1997).
- N.J. Coleman and D.Q.M. Craig, *Int J Pharm* **135**, 13 (1996).
- M. Reading, A. Luget and R. Wilson, *Thermochim Acta* **238**, 295 (1994).
- J.E.K. Schawe, *Thermochim Acta* **261**, 183 (1995).
- Y. Kraftmakher, *Modulation Calorimetry, Theory and Applications* (Springer, Berlin 2004).
- G.P. Johari, *Chem Phys* **258**, 277 (2000).
- S. Brawer, *Relaxation in Viscous Liquids and Glasses: Review of Phenomenology, Molecular Dynamics Simulations, and Theoretical Treatment* (American Ceramic Society, Columbus, OH 1985).
- T.J. Laaksonen and Y.H. Roos, *J Cereal Sci* **33**, 331 (2001).
- C. Faivre, D. Bellet and G. Dolino, *Eur Phys J B* **7**, 19 (1999).
- M. Iza, S. Woerly, C. Danumah, S. Kaliaguine and M. Bousmina, *Polymer* **41**, 5885 (2000).
- A. Ksiazczak, A. Radomski and T. Zielenkiewicz, *J Therm Anal Calorim* **74**, 559 (2003).
- M.R. Landry, *Thermochim Acta* **433**, 27 (2005).
- T. Yamamoto, A. Endo, Y. Inagi, T. Ohmori and M. Nakaiwa, *J Colloid Interface Sci* **284**, 614 (2005).
- C.Y. Yortsos and K.A. Stubos, *Curr Opin Colloid Interface Sci* **6**, 208 (2001).

53. J.N. Hay and P.R. Laity, *Polymer* **41**, 6171 (2000).
54. C. Jallut, J. Lenoir, C. Bardot and C. Eyraud, *J Membr Sci* **68**, 271 (1992).
55. D. Morineau, G. Dosseh, C. Alba-Simionesco and P. Llewellyn, *Philos Mag B* **79**, 1847 (1999).
56. R. Neffati, L. Apekis and J. Rault, *J Therm Anal Calorim* **54**, 741 (1998).
57. M. Sliwinska-Bartowiak, J. Gras, R. Sikorski, R. Radhakrishnan, L. Gelb and E.K. Gubbins, *Langmuir* **15**, 6060 (1999).
58. K.M. Unruh, T.E. Huber and C.A. Huber, *Phys Rev B Condens Matter* **48**, 9021 (1993).
59. M. Wulff, *Thermochim Acta* **419**, 291 (2004).
60. N.V. Churaev, S.A. Bardasov and V.D. Sobolev, *Colloids Surf A Physicochem Eng Asp* **79**, 11 (1993).
61. R. Denoyel and R.J.M. Pellenq, *Langmuir* **18**, 2710 (2002).
62. E.F.J. Esselink, H. van Aalst, M. Maliepaard and J.P.M. van Duynhoven, *Cereal Chem* **80**, 396 (2003).
63. O. Coussy, *J Mech Phys Solids* **53**, 1689 (2005).
64. M. Brun, A. Lallemand, J.-F. Quinson and C. Eyraud, *Thermochim Acta* **21**, 59 (1977).
65. G.W. Scherer, *J Non-Cryst Solids* **155**, 1 (1993).
66. G.W. Scherer, *Cem Concr Res* **29**, 1347 (1999).
67. K. Ishikiriyama and M. Todoki, *J Colloid Interface Sci* **171**, 103 (1995).
68. K. Ishikiriyama, M. Todoki and K. Motomura, *J Colloid Interface Sci* **171**, 92 (1995).
69. G. Cojazzi and M. Pizzoli, *Macromol Phys Chem* **200**, 2356 (1999).
70. K.G. Rennie and J. Clifford, *Faraday Trans I* **73**, 680 (1977).